Polymer Chemistry

PAPER

Cite this: *Polym. Chem.*, 2018, **9**, 3169

Thin cyclomatrix polyphosphazene films: interfacial polymerization of hexachlorocyclotriphosphazene with aromatic biphenols

Evelien Maaskant, [a] Hubert Gojzewski, [b] Mark A. Hempenius, [b] G. Julius Vancso [b] and Nieck E. Benes *[a]

Received 21st March 2018,
Accepted 14th May 2018

DOI: 10.1039/c8py00444g

rsc.li/polymers

A series of thin cyclomatrix polyphosphazene films has been prepared by interfacial polymerization of hexachlorocyclotriphosphazene (HCCP) with an aromatic biphenol. The pK_a values of the biphenol used strongly influence the properties of the hyper-cross-linked films formed. 4,4′-Dihydroxybiphenyl (BPH) and 4,4′-dihydroxydiphenyl ether (DHPE) possess pK_a values in the range of 9.4–9.6 & 10.0–10.3 for the mono- and di-ionized forms, respectively, and produce films with a lower cross-link density, whereas 4,4′-dihydroxybenzophenone (DHBP) and 4,4′-sulfonyldiphenol (BPS) feature lower pK_a values (7.4–7.6 & 8.0–8.2), resulting in films with a higher cross-link density. The difference in cross-link density is reflected in, *e.g.*, the surface morphology and mechanical properties of the films. Mechanical stiffness has been quantitatively assessed by PeakForce QNM AFM. Lower cross-link densities result in Young's moduli with average values of 44–69 MPa, with a sharp distribution, while higher cross-link densities yield broadly distributed Young's moduli with average values of 255–306 MPa, depending on the choice of the biphenol. The surface chemistry of the films was successfully altered by post-functionalization.

1. Introduction

Hybrid materials gained much interest over the last decades, as the combination of organic and inorganic matter within a hybrid material often leads to enhanced, or even novel, properties compared to those of the pure organic and inorganic constituents.[1] For example, hybrid materials may display higher flexibility and greater mechanical strength, usability over a broader temperature range, as well as greater durability.[2] The class of polyphosphazenes holds fascinating examples of inorganic–organic (hybrid) materials.[3] Polyphosphazenes can be regarded as molecular level hybrids as they consist of an inorganic backbone, composed of alternating phosphorous and nitrogen atoms, usually with two organic substituents linked to each phosphorous atom.[4,5] Heteroatoms, such as carbon or sulfur, could be introduced into the polymers backbone resulting in polyheterophosphazenes.[6–8] Besides linear polyphosphazes, star, dendritic, block copolymeric, cyclolinear, and cyclomatrix architectures have been synthesized.[9,10]

A versatile building block for the preparation of materials based on phosphazenes is the cyclic phosphazene trimer hexachlorocyclotriphosphazene $[NPCl_2]3$, HCCP. Covalent linkages can be formed between nucleophiles, such as alkylamines, and the phosphorous atoms, with chloride as the leaving group. In cyclolinear polymers, only two of the six reactive sites of the phosphazene rings are linked *via* difunctional exocyclic groups to form linear chains. When a larger number of reactive sites are involved in bond formation, cyclomatrix structures result, which are cross-linked materials. Precipitation polycondensation reactions under such conditions (where multiple HCCP sites reacted with organic small molecules, or polymers having at least two hydroxyl or amine groups) have yielded cyclomatrix polyphosphazene microspheres.[11] These cyclomatrix materials are mainly known for their excellent flame retardant properties,[12,13] but are also used for biocompatible coatings,[14] sensing applications,[15] adhesives,[16] or super-hydrophobic coatings.[17] Aromatic organic building blocks were commonly used, though aliphatic diamines[18] or polymers[11] were reported as well.

Conventional methods to prepare films, *e.g.*, doctor-blade casting, drop casting, or spin coating result in relatively thick films in the order of a few hundred microns. Here, we have

[a]*Films in Fluids Group - Membrane Science and Technology cluster, Faculty of Science and Technology, MESA+ Institute for Nanotechnology, University of Twente, P.O. Box 217, 7500 AE Enschede, The Netherlands. E-mail: n.e.benes@utwente.nl*
[b]*Materials Science and Technology of Polymers, Faculty of Science and Technology, MESA+ Institute for Nanotechnology, University of Twente, P.O. Box 217, 7500 AE Enschede, The Netherlands*

prepared thin films of a cyclomatrix polyphosphazene material by interfacial polymerization (IP). IP most often involves a polycondensation reaction of two or more monomers at the interface of two immiscible phases. When at least one of the monomers has a higher functionality than two, an insoluble thin cross-linked film is formed at the interface. These films possess much higher stability in aggressive environments compared to their uncross-linked analogues. Due to the localized nature of the reaction, thin, defect-free films could be obtained.[19–21]

Interestingly, IP has been successfully employed in the preparation of several HCCP-based molecules. Thompson *et al.*[22] achieved selective di-substitution of HCCP with bisphenol A, yielding di(bisphenol A)-tetrachlorocyclotriphosphazene. Chen-Yang *et al.*[23] prepared mono- through hexa-substituted (phenoxy)cyclotriphosphazenes by interfacial condensation of HCCP with phenol. These authors showed that the highest reaction rates could be obtained using chlorinated solvents, which reduce the hydrolysis of HCCP chlorine groups upon contact with water, due to the low solubility of water in these media.

Here we report, to our knowledge, on the first examples of cyclomatrix thin (2–5 μm) polyphosphazene films prepared by IP (Fig. 1). These films were obtained by the interfacial polycondensation of HCCP with the aromatic biphenols 4,4′-dihydroxybiphenyl (BPH), 4,4′-dihydroxydiphenyl ether (DHPE), 4,4′-dihydroxybenzophenone (DHBP), and 4,4′-sulfonyldiphenol (BPS). We note, that cyclomatrix polyphosphazenes based on BPS are well described in the literature when prepared in a single solvent.[24–28]

The chemical structure of the aromatic biphenol has a strong influence on the stiffness (Young's modulus) and thermal stability of the corresponding thin film, originating from differences in the cross-link density. The properties of the final films seem to depend strongly on the pK_a values of the aromatic biphenol used. Judicious selection of the aromatic biphenol therefore allows facile tuning of the properties of the cyclomatrix thin polyphosphazene film.

2. Experimental

2.1. Materials

Phosphonitrilic chloride trimer (HCCP, 99%), sodium hydroxide (NaOH, >98%), dichloromethane (DCM, ACS reagent, ≥99.5%), 4,4′-dihydroxybiphenyl (BPH, 97%), 4,4′-dihydroxybenzophenone (DHBP, 99%), 4,4′-sulfonyldiphenol (BPS, 98%), tricaprylylmethylammonium chloride (Aliquat® 128), and 2,2,2-trifluoroethanol (TFE, ≥99.0%) were obtained from Sigma-Aldrich (the Netherlands). 4,4′-Dihydroxydiphenyl ether (DHPE, >98%) was obtained from TCI Europe. Sylgard 184 was obtained from DOW-Corning. All chemicals were used as received.

2.2. Preparation of hyper-cross-linked polyphosphazenes

The reaction conditions of the interfacial polycondensation of HCCP with an aromatic biphenol are based on the work of Chen-Yang *et al.*[23] HCCP (0.70 g, 2 mmol) and Aliquat® 128 (a phase transfer catalyst) (0.42 g, 1 mmol) were dissolved in DCM (20 mL). Biphenol (10 mmol) and NaOH (1.6 g, 40 mmol) were dissolved in Milli-Q water (20 mL). The aqueous phase was added to the organic phase, and the mixture was stirred vigorously for 10 minutes. The formed suspension was filtered and washed with water and ethanol, respectively, and dried in a vacuum oven at 60 °C overnight. The resulting solid was ground to a fine powder. Unreacted monomers and impurities were extracted with ethanol in a Soxhlet apparatus. The remaining solids were dried under vacuum.

2.3. Thin polyphosphazene films on PDMS slabs

A 1 cm thick PDMS layer was casted in a petri dish using Sylgard 184 (DOW-Corning). Both Sylgard components were mixed according the manufacturer's instructions, and centrifuged at 4000 rpm for 15 minutes to remove air bubbles. The PDMS was poured in a petri dish and cured at 80 °C for 3 hours. A piece of PDMS was soaked into the DCM-phase (same composition as described above) for at least 10 minutes. The swollen PDMS was put on a piece of paper to remove the excess DCM from the surface, and immediately placed in the aqueous phase (same composition as described above) for 5 minutes to allow for film formation at the PDMS surface. The PDMS slabs were dipped in Milli-Q water to remove any unreacted monomers. See Fig. 2 for a schematic representation of the synthesis procedure. After drying overnight at ambient conditions, the HCCP-biphenol film could be easily removed from the PDMS surface. After removal from the PDMS, the films were washed with water and ethanol, respectively.

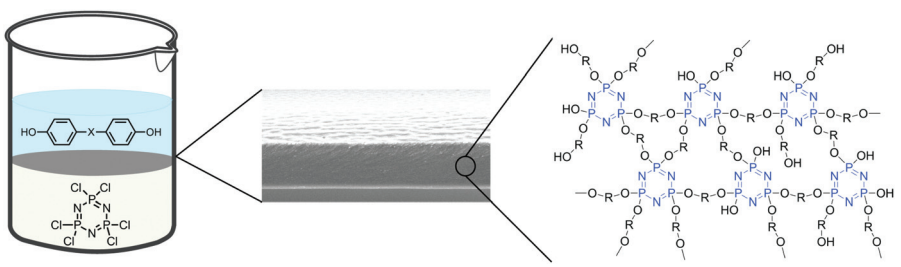

Fig. 1 The preparation of cyclomatrix polyphosphazenes by interfacial polymerization.

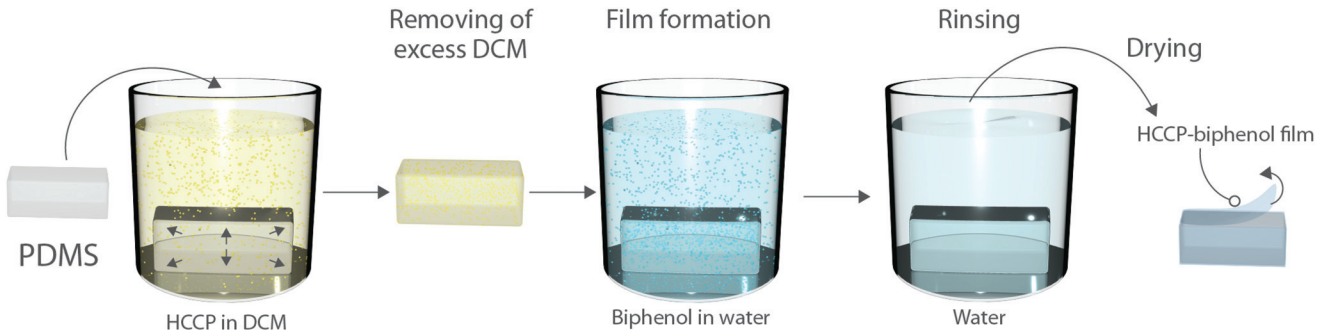

Fig. 2 Preparation of hyper-cross-linked polyphosphazene films on the surface of PDMS slabs. A PDMS slab is soaked into the organic phase containing the monomer HCCP, and a phase transfer catalyst Aliquat® 128. Note that the organic phase used here (DCM) has a higher density than the aqueous one. The excess DCM is removed from the surface of the PDMS. The swollen slab of PDMS is immediately placed in the aqueous phase. A thin film is formed at the surface of the PDMS due to the solvents' immiscibility. After 5 minutes reaction time, the PDMS slab is removed from the aqueous solution, dipped immediately in water, and dried overnight at ambient conditions. During drying the DCM evaporates, and the PDMS will slowly return to its original shape. Due to this gradual shrinkage of the support, the HCCP-biphenol film does not tear upon drying. The film is not covalently bound to the PDMS and can be easily removed with tweezers.

2.4. Post-functionalization of HCCP-biphenol films

Immediately after their synthesis, PDMS slabs containing a HCCP-biphenol film were submerged for 5 minutes in an aqueous solution (20 mL) of TFE (2 g, 20 mmol) and NaOH (1.6 g, 40 mmol). After a reaction time of 5 minutes, the films were washed with water, and dried at ambient conditions overnight.

2.5. Characterization

FTIR-ATR spectra were recorded on an ALPHA spectrometer equipped with an ATR platinum diamond crystal (Bruker, Germany). The powders were pressed onto the ATR crystal without further sample preparation. Spectra were averaged over 64 scans with a resolution of 4 cm^{-1}. Prior to measurements, a background spectrum was recorded at ambient conditions.

Scanning electron micrographs and energy dispersive X-ray spectra were taken with a JEOL-JSM6010 scanning electron microscope. Samples were coated with a 5 nm chromium layer (Quorum Q150 T ES) prior to imaging. Film thicknesses were measured using the image processing program ImageJ (v1.50) software.

Quantitative mapping of Young's modulus and adhesion force by atomic force microscopy (AFM) was performed on HCCP-biphenol films.[29,30] Films were fastened using a two-component epoxy glue to a metal sample holder and left for 24 h to cure the epoxy. Specimens were measured in the PeakForce QNM (Quantitative Nanomechanical Mapping) working mode using the Multimode 8 AFM controlled by the NanoScope V control unit (Bruker, USA). Soft ScanAsyst-Air (Bruker, USA) silicon nitride cantilevers with a nominal spring constant of 0.4 N m^{-1} and sharp silicon tips with a nominal tip-end radius of 2 nm were used to ensure damage-free tip–sample interactions. The value of the individual cantilever spring constant was determined by the thermal tune method;[31,32] we obtained values ranging within 0.31–0.39 N m^{-1} depending on the cantilever. In the AFM mode used, sample topography and structure–property relationships are obtained by real-time processing of the force–distance curves. Force–distance curves were captured each time the tip tapped on the specimen surface, *i.e.* at each pixel; 65 536 force–distance curves were collected (256 × 256 pixels) for each AFM image, which yielded "elasticity maps". The tip followed a 2 kHz sine-wave trajectory when moving from one pixel to another with a peak-force amplitude of 150 nm. Imaging was performed in air, at controlled temperature (21.0 ± 0.1 °C) and stable values of relative humidity (40%). Image processing and data evaluation were performed with the NanoScope 8.15 and NanoScope Analysis 1.80 software, respectively. The ScanAsyst panel in the NanoScope 8.15 software was set to be off to minimize the influence of software auto-optimization algorithms on the data collected.

Young's modulus calculations were performed based on the model of Derjaguin, Muller, and Toporov (DMT)[33,34] and the following formalism was employed assuming a rigid AFM tip:

$$E = (F_L - F_{adh})\frac{3(1-\nu^2)}{4}R^{-1/2}(z-d)^{-3/2} \quad (1)$$

where: E is the sample's Young's modulus, F_L is the applied load through the AFM tip against the sample surface, F_{adh} is the adhesion force between the sample surface and the tip, with ν sample Poisson's ratio, R radius of curvature of theAFM tip, z the position of the AFM scanner, and d the cantilever deflection. To perform real-time data analysis and reduce the propagation of errors, we applied a simplified formalism of the DMT model to calculate Young's modulus, which is referred to as the "relative method".[30,35,36] Here, the value of the sample Poisson's ratio and radius of curvature of the AFM tip were no longer required, as the values of the Young's moduli were determined using a references sample with known DMT elastic modulus. As reference, we employed a PDMS gel 150 μm film with a Young's modulus of (3.5 ± 0.5 MPa) (Bruker).[35,37] The adhesion force was calculated as the differ-

ence between the baseline and the snap-off point (the lowest point in the force–distance curve). The distribution of the Young's modulus was plotted as histogram, where the bin width was determined using Scott's normal reference rule.[38]

XPS (X-ray Photoelectron Spectroscopy) measurements were carried out on HCCP-biphenol films. XPS spectra of HCCP-BPH, HCCP-DHPE, and HCCP-DHBP films were measured on an Ultra Axis™spectrometer (Kratos Analytical, Manchester UK). The films were irradiated with mono energetic Al $K_{\alpha 1.2}$ radiation (1486.6 eV) and the spectra were taken at a power of 144 W (12 kV × 12 mA). The XPS spectrum of the HCCP-BPS film was measured on a Quantera SXM scanning XPS microprobe (Physical Electronics). The films were irradiated with monochromatic Al K_{α} radiation (1486.6 eV) with a beam size of 200 μm at a power of 50 W. Fitting of all spectra was done after shifting the measured spectra with respect to the known reference binding energy of aliphatic carbon C 1s at 284.8 eV.

Streaming current measurements were performed on a SurPASS analyzer (Anton Paar, Austria) equipped with an adjustable gap cell. HCCP-biphenol films were fastened to the PDMS blocks (2 × 1 cm^2) of the cell with double sided adhesive tape (Tesa® 4965). The pH of the electrolyte solution (5 mM KCl) was automatically adjusted using 0.1 M HCl or 0.1 M NaOH. From the streaming current, the zeta potential could be derived using (2):

$$\zeta = \frac{dI}{dP} \cdot \frac{\eta}{\varepsilon \cdot \varepsilon_0} \cdot \frac{L}{A} \quad (2)$$

where: ζ is the zeta potential, $\frac{dI}{dP}$ is the slope of the streaming current *versus* pressure, η and ε are the viscosity and dielectric constant of the electrolyte, here taken as that of water, ε_0 is the permittivity of vacuum, L is the length of the streaming channel, and A is the cross sectional area of the channel.

Combined thermogravimetric analysis (TGA) and mass spectroscopy (MS) measurements were performed on HCCP-biphenol powders using an STA 449 F3 Jupiter TGA with an aluminum sample cup (Netzsch, Germany) and QMS 403 D Aeolos MS (Netzsch, Germany). The methods used for these measurements are described elsewhere.[39] Mass loss measurements were performed from 50 to 600 °C with a heating rate of 10 °C min^{-1} under nitrogen atmosphere. Isothermal analysis was performed at 600 °C with a heating rate of 10 °C min^{-1} under nitrogen atmosphere.

Differential scanning calorimetry (DSC) curves were obtained using a PerkinElmer DSC 8000 at a heating and cooling rate of 20 °C min^{-1} under a nitrogen atmosphere.

3. Results and discussion

3.1. Synthesis of hyper-cross-linked polyphosphazenes

Cyclomatrix hybrid polyphosphazene powders and thin films were prepared by interfacial polymerization of the inorganic monomer HCCP and an aromatic biphenol. The interfacial polymerization of two monomers where one of the monomers has a high functionality (≥3) results in an insoluble network at the interface of two immiscible phases. In contrast to the preparation in a single solvent, interfacial polymerization allows for the localized formation of highly cross-linked thin films with a perfectly alternating monomeric structure. To distinguish from conventional cross-linked polymers, we will denote these networks made by interfacial polymerization as hyper-cross-linked.

Scheme 1 shows the molecular structure of the biphenols used in this study, where a schematic representation of the reaction with HCCP is also displayed. The hydroxyl groups of the biphenols are deprotonated by NaOH to form the reactive biphenol dianions, and to make the aromatic biphenols soluble in the aqueous phase. Table 1 shows the pK_{a1} and pK_{a2} values of the biphenols used in this study, where pK_{a1} refers to the first deprotonation and pK_{a2} to the second deprotonation. The pH value of the aqueous solution was approximately 13.3, independent of the biphenol used.

Successful network formation relies on the high conversion of the biphenols into dianions, as these species possess a much higher nucleophilicity than the parent biphenols. Complete deprotonation ensures the formation of full dianio-

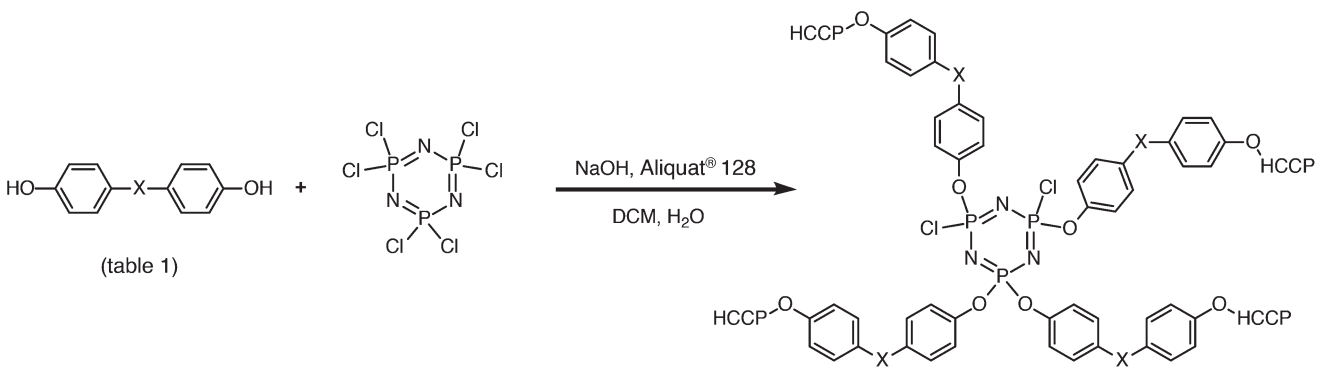

Scheme 1 Schematic representation of the reaction at the interface of the aqueous and organic phases. The structures of the aromatic biphenols used are shown in Table 1. First, the aromatic biphenol is converted to its more reactive sodium aryloxide by sodium hydroxide, followed by nucleophilic substitution with the HCCP monomer.

Table 1 The chemical structure and pK_a values of the aromatic biphenols used in this study

Biphenol	Structure	pK_{a1}[a]	pK_{a2}[a]
BPH	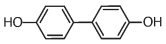	9.64	10.32
DHPE	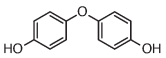	9.40	10.00
DHBP	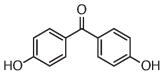	7.55	8.16
BPS	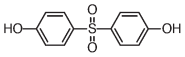	7.42	8.03

[a] Obtained from Chemicalize.com (ChemAxon).[40]

nic functionality of these reactants. The BPH and DHPE monomers contain electron donating groups that make these aryloxide anions more nucleophilic, and thus more reactive. However, due to the higher pK_a of these biphenols, there is a higher chance of incomplete deprotonation, *i.e.* of the presence of monoanions among the biphenol dianions. In contrast, the hydroxyl groups of DHBP and BPS are significantly more acidic than those of BPH and DHPE, due to the electron-withdrawing carbonyl and sulfonyl moieties, and are therefore expected to be ionized into dianions more readily by the employed base than BPH and DHPE. It is well known that the degree of dissociation of acids is determined by the difference between the pH of the employed base solution and the pK_a of the acid.[41] We note here, that as we show later, biphenol acidity can be correlated directly with the cross-link density of the formed networks.

At the interface of the aqueous phase (biphenol) and the organic phase (HCCP), a sodium aryloxide ion displaces one of the chlorine groups of HCCP to form a P–O–C bond. Due to the high functionality of HCCP, an insoluble hyper-cross-linked network is formed. In addition to these HCCP-biphenol thin films, HCCP-biphenol powders were prepared by vigorously stirring a mixture of both the aqueous phase and the organic phase. Fig. 3 shows the FTIR spectra of these HCCP-biphenol powders. All samples show absorbance peaks around 1590 cm^{-1} and 1490 cm^{-1} belonging to the C=C stretching vibrations of the phenyl rings. The broad band from 1200–1120 cm^{-1}, with a peak at 1150 cm^{-1}, originates from the asymmetric P=N–P stretching, while the peak at 870–880 cm^{-1} belongs to the symmetric P=N–P stretching.[25,26,42] The absorbance peak at 940 cm^{-1} originates from the P–O–Ph bond, indicating the successful preparation of a cross-linked network for all aromatic monomers used.

The absorption band of the ether group in the DHPE biphenol is not visible in the spectrum of HCCP-DHPE since this band overlaps with the broad band belonging to the P=N–P ring stretching present at 1200–1120 cm^{-1}. The spectrum of HCCP-DHBP shows a strong absorption band at 1650 cm^{-1} due to the carbonyl stretching of the ketone group of the DHBP biphenol. The sulfone group of the BPS monomer gives rise to a strong absorption peak at 1290 cm^{-1}. The second absorption band of the sulfone group overlaps with the P=N–P stretching (1150 cm^{-1}) of the HCCP monomer.[25,26]

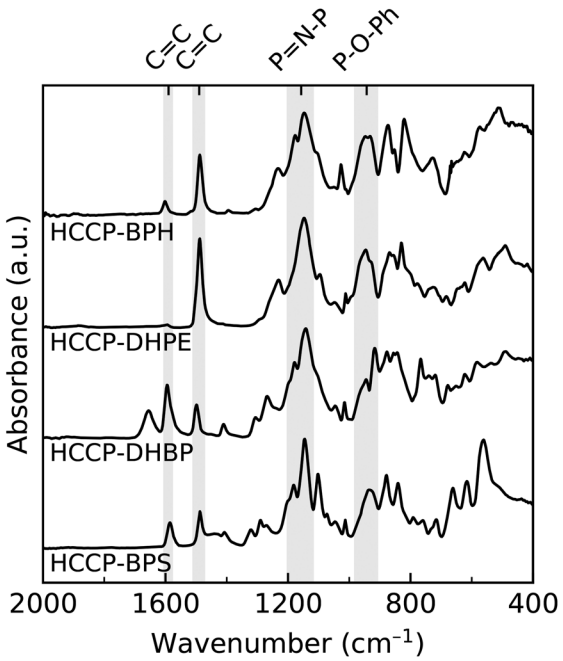

Fig. 3 FTIR spectra for HCCP-biphenol powders from 2000–400 cm^{-1}.

3.2. Surface morphology and mechanical properties

Thin polyphosphazene films were prepared by interfacial polymerization onto the outer surface of the PDMS slabs (Fig. 2). We note that the use of PDMS as support for interfacial polymerization reduces the mechanical stresses in the films upon drying, thus preventing cracking. Following completion of the reaction, the films can be easily peeled of the PDMS support, to obtain free-standing hyper-cross-linked polyphosphazene films. Cross-sectional scanning electron micrographs of HCCP-biphenol films prepared onto PDMS are shown in Fig. 4, and top view scanning electron micrographs are shown in Fig. 5. The HCCP-BPH and HCCP-DHPE films possess a relatively rough surface on a macroscopic scale (Fig. 5a–d), while HCCP-DHBP and HCCP-BPS possess a smoother surface (Fig. 5e–g). Due to contributions of surface roughness, the thickness values of HCCP-BPH vary between 2 and 5 μm, and the thickness of HCCP-DHPE varies between 3 μm and 5 μm over the entire cross-section of the films. In contrast, HCCP-DHBP and HCCP-BPS have a very uniform thickness over the entire cross-section of ~3.4 μm and ~3.5 μm, respectively.

The surface morphology of a film derived by interfacial polymerization is strongly dependent on the diffusivity and the solubility of the monomers into the other phase.[43,44] The rough surface morphology of HCCP-BPH and HCCP-DHPE films is typically obtained when one of the reactants easily diffuses through the forming film to the reaction site. Zhang *et al.*[45] found a similar trend when studying the film formation

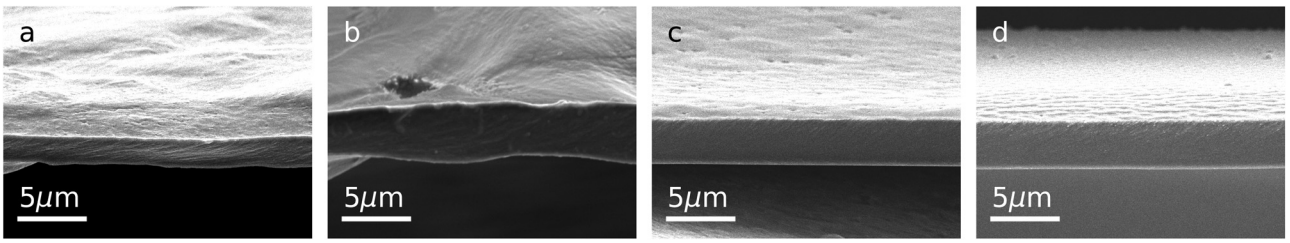

Fig. 4 Cross-sectional scanning electron micrographs of HCCP-biphenol films. (a) HCCP-BPH, (b) HCCP-DHPE, (c) HCCP-DHBP, and (d) HCCP-BPS.

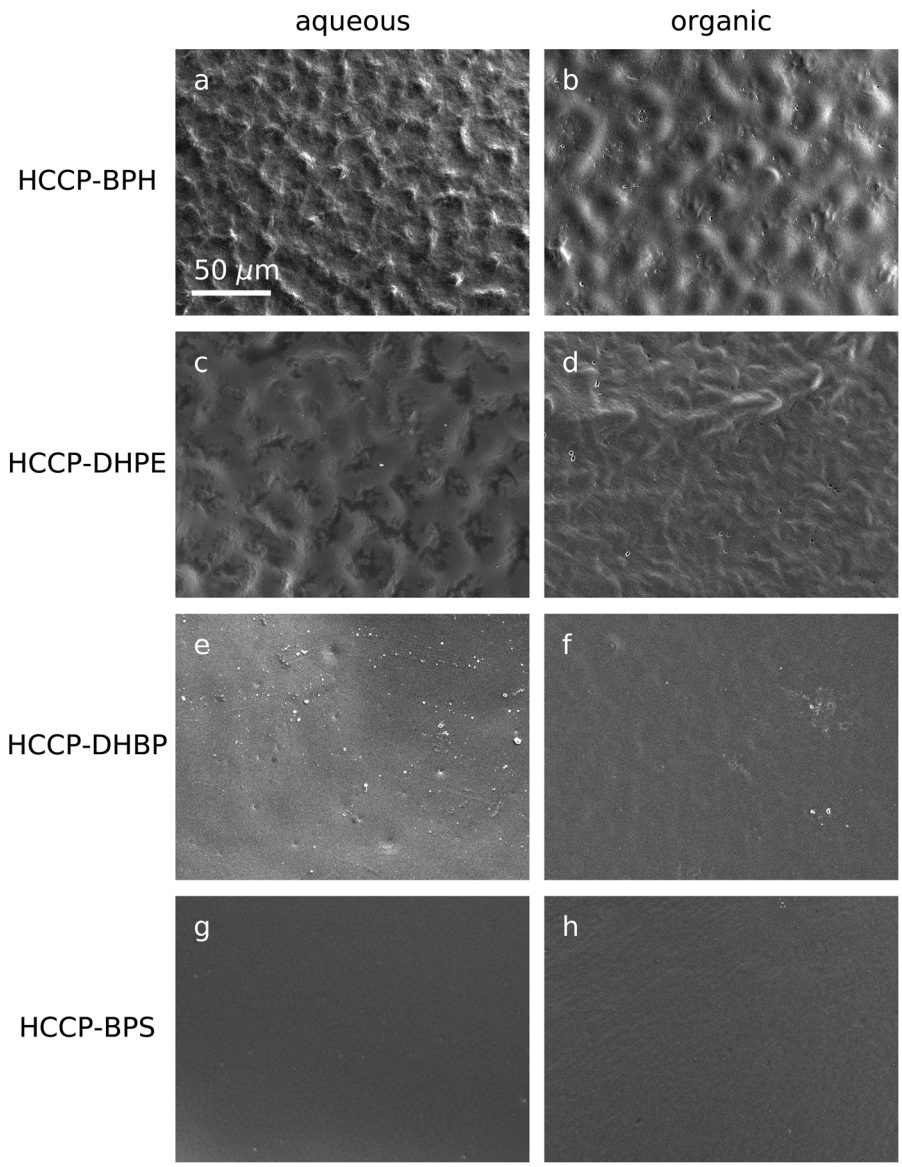

Fig. 5 Top view scanning electron micrographs of the HCCP-biphenol films prepared by interfacial polymerization onto PDMS. (a) HCCP-BPH aqueous side, (b) HCCP-BPH organic side, (c) HCCP-DHPE aqueous side, (d) HCCP-DHPE organic side, (e) HCCP-DHBP aqueous side, (f) HCCP-DHBP organic side, (g) HCCP-BPS aqueous side, and (h) HCCP-BPS organic side. HCCP-BPH and HCCP-DHPE form a relatively rough film whereas HCCP-DHBP and HCCP-BPS have a smooth surface.

of various amines with trimesoyl chloride. In contrast, HCCP-DHBP and HCCP-BPS films reveal a smooth surface morphology. This can indicate that the diffusion of monomers through the forming film was more limited resulting in smoother film. Since the sizes of the aromatic biphenols are rather similar, the limited diffusion could be explained by a more tightly cross-linked network in the case of HCCP-DHBP and HCCP-BPS. As can be seen from Fig. 5, the surface morphology does not strongly differ for the aqueous-phase or organic-phase side for all the films.

The difference in cross-link density, which depends on the employed biphenol, is of influence on the mechanical properties of the final films. As earlier mentioned, we used the PeakForce QNM mode to characterize the morphology and mechanical properties (Young's modulus and adhesion force) of HCCP-biphenol films. Fig. 6 shows the results of these AFM measurements for all HCCP-biphenol films, for 3 μm × 3 μm scan size images. Height (topography) and Young's modulus are presented with corresponding cross-section plots (obtained along the white lines in the images). The cross-section profile in the height images shows no significant differences among the aromatic monomers BPH, DHPE, and DHBP (Fig. 6a–c); the height varies in the range of 20 nm for these films. For HCCP-DHBP we observed a grain-like morphology. The grain-like features have a size of approximately 200 nm in diameter and several nm in height. The HCCP-BPS film (Fig. 6d) reveals

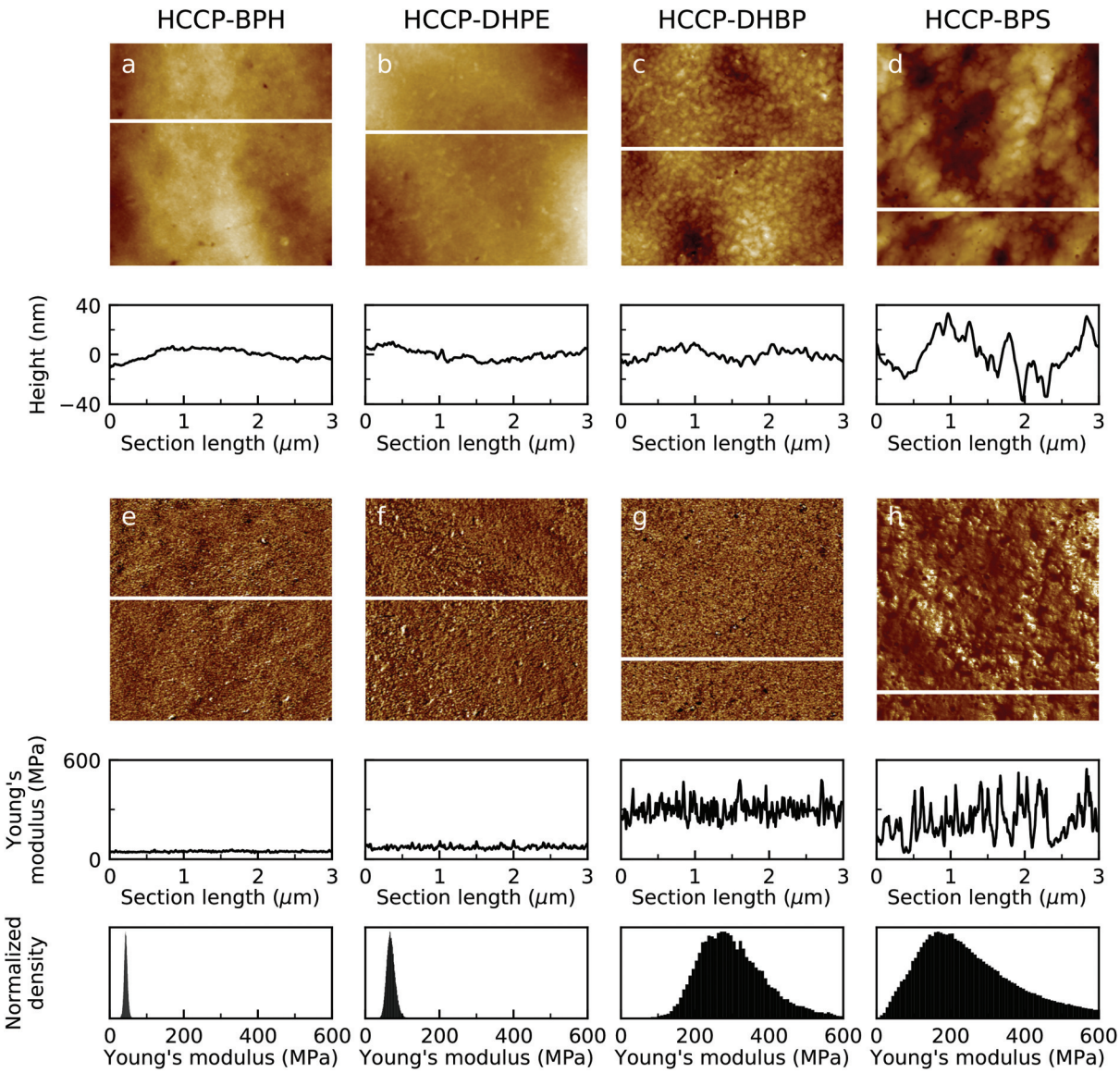

Fig. 6 AFM quantitative characterization: topographical (a, b, c, and d) and Young's modulus (e, f, g, and h) images (3 μm × 3 μm) for the organic side of HCCP-BPH, HCCP-DHPE, HCCP-DHBP, and HCCP-BPS films. Height and Young's modulus profiles (cross-sections) of the samples were taken along the white lines shown. The corresponding distributions of Young's moduli are shown as histograms (obtained from all force–distance curves per map).

Table 2 The surface roughness and Young's modulus of HCCP-biphenol films calculated from the peak force tapping data

		Young's modulus (MPa)		
Sample	R_{RMS} [a] (nm)	Mean[b]	Median	Mode
HCCP-BPH	0.9	44 ± 5	43	44
HCCP-DHPE	1.2	69 ± 12	68	66
HCCP-DHBP	2.3	306 ± 98	292	321
HCCP-BPS	8.7	255 ± 140	227	182

[a] Root-mean-square surface roughness (R_{RMS}) from 0.5 μm × 0.5 μm surface areas. [b] Error represents the standard deviation from the mean.

height variations of up to 80 nm. The differences in height profile are also reflected in the surface roughness, *i.e.* the R_{RMS}, as shown in Table 2.

The Young's modulus maps of the films are shown in Fig. 6e–h. All films show a rather homogeneous distribution of Young's moduli over the imaged surfaces. This fits well with the notion that the network features a rather homogeneous structure down to the molecular scale.

The average Young's modulus of the HCCP-DHBP (306 ± 98 MPa) and HCCP-BPS (255 ± 140 MPa) films is significantly different compared to that of the HCCP-BPH (44 ± 5 MPa) and HCCP-DHPE (69 ± 12 MPa) films. The modulus distribution also shows variations for the different samples. The higher average Young's modulus of HCCP-DHBP and HCCP-BPS can be explained by a higher cross-link density due to the lower pK_a values, and thus more complete ionization into dianions, of the biphenols used to obtain the films. The significant standard deviation in the Young's modulus distribution could be caused by variation of tip-film contact area due to an enhanced surface roughness. The broad distribution could also be caused by local modulus heterogeneities, due to differences in cross-link densities, but this argument remains speculative due to lack of data.

The adhesion force maps (not shown) unveiled homogeneous distribution. The adhesion force value distributions are very narrow and exhibit average values within the range of 0.3–4.0 nN for all samples. Taking into account the nominal radius of the AFM tip (2 nm), this can be converted into a tip-normalized adhesion ranging between 0.15 to 2.0 N m^{-1}. The low values of the tip-normalized adhesion for HCCP-BPH, HCCP-DHPE, and HCCP-DHBP confirm that the surfaces of the films are hydrophobic, especially in the case of the rigid HCCP-DHBP films, as the capillary force contributions between the AFM tip and films seem to be greatly reduced.[46,47] The HCCP-BPS films show a much higher tip-normalized adhesion, indicating the more hydrophilic character of the film, originating from the sulfonyl-groups.

3.3. Surface composition and charge

Table 3 shows the atomic composition of the surface of HCCP-biphenol films measured by XPS. Besides the atoms present in HCCP and the aromatic biphenol (C, N, O, P, Cl, S) there are some traces of Si and Na present at the surface of some of the films. Traces of Si are most likely due to the usage of the PDMS slabs. The traces of Na can be either from the presence of unreacted sodium aryloxide groups, or from the formation of NaCl during the condensation reaction. The Cl (2p) peak for HCCP-DHPE and HCCP-DHBP can be fitted with two peaks, where one could be fitted with a peak having a maximum at 198.7 eV, that corresponds to the binding energy of NaCl.[48]

The number of reacted chlorine groups at the surface of the film can be calculated from various atomic ratio's. Since the atomic percentages of O and Cl can be influenced by the hydrolysis of P–Cl to P–OH in the presence of H_2O, and by the presence of NaCl entrapped in the network, only the number of reacted chlorine groups based on the ratio's C/N and C/P is reported. In general, the number of reacted chlorine groups of HCCP at the surface matches relatively well to the results obtained by AFM; HCCP-DHBP and HCCP-BPS possess a higher modulus, and are therefore more cross-linked. Again, we want to emphasize that this is a surface property, and cannot be correlated with bulk properties.

All films show a rather similar surface charge, independent of cross-link density. Fig. 7 shows the zeta potential of HCCP-biphenol films as a function of pH. The isoelectric point (IEP), *i.e.* the pH where the net surface charge is zero, was independent of the biphenol used. The HCCP-BPH film has an IEP of 5.0, HCCP-DHPE of 4.6, HCCP-DHBP of 4.5, and HCCP-BPS of 4.8. The films have a highly negatively charged surface at pH values higher than the IEP. Zhou *et al.*[14] and Chen *et al.*[49] reported the zeta potential of HCCP-BPS microshperes in

Table 3 Atomic composition and number of reacted chlorine groups at the surface of the HCCP-biphenol films obtained from XPS measurements. Atomic percentage values were calculated by the Gaussian fit to the XPS spectra

	Atomic composition (%)								Reacted Cl groups[a]	
Sample	C (1s)	N (1s)	O (1s)	P (2p)	Cl (2p)	S (2p)	Na (1s)	Si (2p)	C/N	C/P
HCCP-BPH	73.76	5.26	10.44	4.15	4.13	—	—	2.25	3.5	4.4
HCCP-DHPE	64.50	5.18	17.72	4.66	4.82	—	0.66	2.42	3.1	3.5
HCCP-DHBP	71.61	3.61	15.68	2.90	3.21	—	1.78	1.20	4.6	5.7
HCCP-BPS[b]	56.13	4.63	23.53	4.41	1.56	3.19	—	6.46	3.0	2.9

[a] The number of organic biphenols per HCCP molecule, *i.e.* the number of reacted Cl groups, calculated using the atomic ratios C/N or C/P. [b] This sample was measured with a different XPS apparatus.

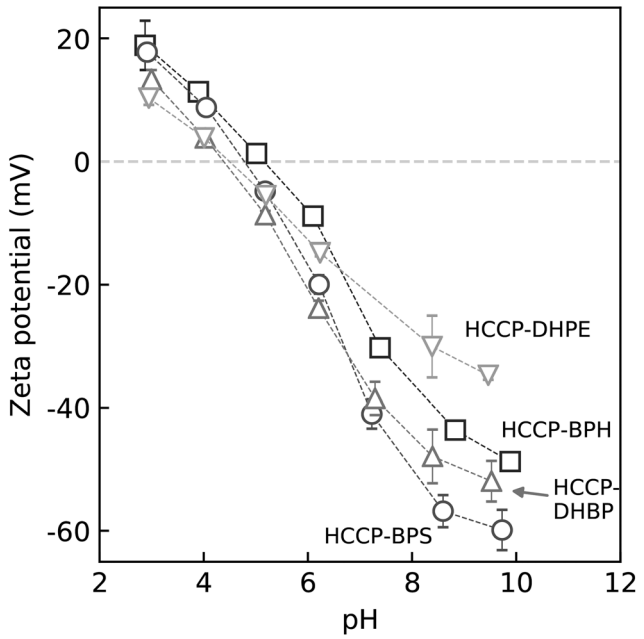

Fig. 7 Zeta potential as function of pH for HCCP-BPH (□), HCCP-DHPE (▽), HCCP-DHBP (△), and HCCP-BPS (○). The error bars represent the 95% confidence interval, calculated from four data points.

water in the same range as our data. The authors attribute this negative surface charge to the deprotonation of protuding phenolic hydroxy groups. Since the pK_a of all biphenols used is much higher than the experimentally found IEP, there must be another functional group contributing to the IEP of the HCCP-biphenol films. As mentioned before, unreacted P–Cl bonds can hydrolyze to P–OH bonds. Therefore, we attribute the low IEP to the presence of these P–OH groups. Calculating the pK_a of several substituted (phenoxy)hydroxycyclotriphosphazenes using Chemicalize confirms this assumption.[40] At higher pH, the HCCP-DHBP and HCCP-BPS films are more negatively charged compared to the HCCP-BPH and HCCP-DHPE films. This effect can be attributed to the pK_a of the phenolic hydroxy groups. DHBP and BPS possess a significantly lower pK_{a1}, and therefore contribute to the surface charge at lower pH, resulting in a lower total surface charge compared to BPH and DHPE at the same pH.

3.4. Thermal properties

The thermal properties of HCCP-biphenol powders were characterized with DSC and TGA-MS. None of the powders showed a glass transition temperature in the DSC traces. This confirms the hyper-cross-linked nature of these materials.

Due to the incorporation of an inorganic monomer and the use of fully aromatic organic compounds, the HCCP-phenol networks show excellent thermal stability with mass loses of less than 25% after a two hour dwell at 600 °C under nitrogen atmosphere. This has been observed for all networks, except HCCP-BPS that shows a mass loss of 40% due to the less thermally stable sulfone group. Fig. 8a shows the mass loss of HCCP-biphenol powders during heating to 600 °C with a heating rate of 10 °C min^{-1}. Fig. 8b shows the mass loss during an isothermal phase at 600 °C. The gases evolved during heating were analyzed by a mass spectrometer as shown in Fig. 8c–f.

The first fragments were detected starting at temperatures around 100 °C, with a peak around 200 °C for all powders. Mainly fragments of C_3H_3 and CO_2 evolved at this stage, although small traces of H_2O and HCl were detected as well. The release of these fragments, except HCl, is related to the decomposition of the organic biphenol. These decomposition fragments can originate from unreacted organic monomers entrapped in the network, as well as the thermal conversion of some P–O–C bonds to the more stable P–O–P bonds. The latter results in the release of the organic cross-linker, and would contribute to further cross-linking to ultimately produce a completely inorganic network.[50,51] The minor loss of HCl can originate from further reaction of HCCP with unreacted biphenols.

Above 300 °C (400 °C for HCCP-BPS) a significant release of HCl is detected, followed by the release of C_3H_3 at temperatures above 450 °C. The significant release of HCl can be explained by the decomposition of P–Cl bonds. Due to the hyper-cross-linked nature of the material, unreacted P–Cl bonds are present. This is caused by highly cross-linked nature of the material; the nucleophile such as a biphenol, or even water, is not able to reach all the reactive sites within the network. The release of C_3H_3 above 450 °C proves that the material is still hybrid in nature at this temperature, despite partial decomposition of the biphenol at lower temperatures.

All networks show the same trends regarding the fragments that are released upon heating and only minor differences are found when considering in more detail. HCCP-BPH shows barely any release of aromatic fragments at temperatures above 450 °C due to the fully aromatic structure of the biphenol, whereas HCCP-DHPE and HCCP-DHBP have an ether or a ketone linker, respectively; slightly reducing the thermal stability at elevated temperatures. Introducing a sulfone group greatly reduces the stability of the biphenol, and thus the network, as can be concluded from Fig. 8f.

The release of HCl and SO_2 has the highest contribution to the overall mass loss of the powders when considering the peak area of the MS signal. The release of HCl can be related to the cross-link density of the material. Of all biphenols, HCCP-DHBP shows the smallest release of HCl relative to the CO_2 signal, which corresponds well to the cross-link density and the highest residual mass. Note that the area of the peaks among the samples is not directly comparable due to the difference in absolute sample mass.

In contrast, HCCP-BPS shows the lowest residual mass. This is mainly caused by the decomposition of the bisphenol S biphenol, as proven by the release of SO_2. The significant mass loss at 500 °C and the residual mass of 60% at 600 °C corresponds well to the findings of Chen-Yang *et al.*[52] for the chemically similar cyclolinear polymer. The performance of these thin cross-linked polymer films clearly matches that of their

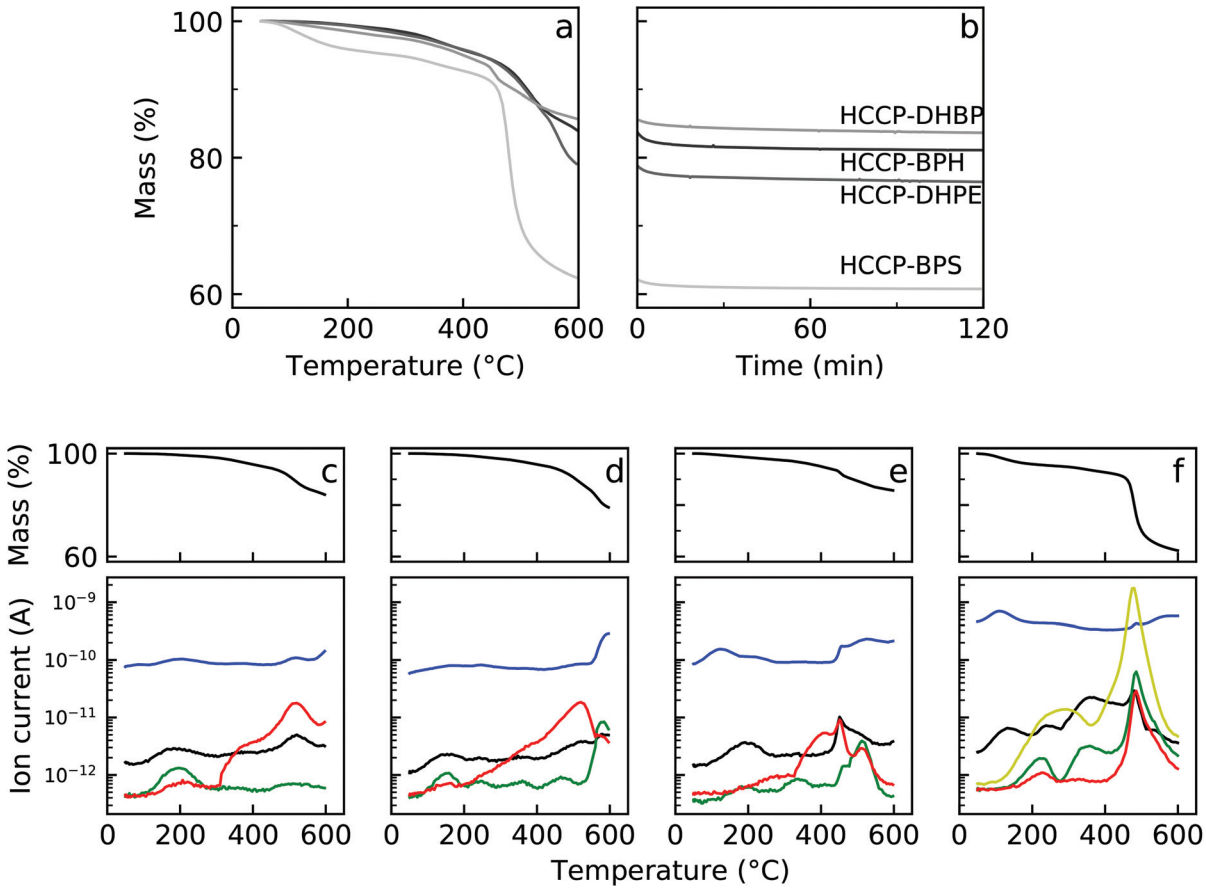

Fig. 8 (a) Mass loss up to 600 °C as function of temperature for HCCP-biphenol powders under nitrogen atmosphere, obtained with a heating rate of 10 °C min^{-1}. (b) Mass loss as a function of time at 600 °C for 2 hours showing that after an initial mass loss upon heating, the mass is stabilized. (c–f) The mass loss (top) and mass spectrometer signal (bottom) upon heating for (c) HCCP-BPH, (d), HCCP-DHPE, (e) HCCP-DHBP, and (f) HCCP-BPS. The release of H_2O (m/z = 18, blue, —), HCl (m/z = 37, red, —), C_3H_3 (m/z = 39, green, —, fragment of aromatic rings), CO_2 (m/z = 44, black, tbf—), and SO_2 (m/z = 64, yellow, —) is shown as function of temperature.

linear bulk analogues, thus demonstrating the potential of the interfacial fabrication method.

3.5. Post-functionalization of HCCP-biphenol films

The HCCP-biphenol films have unreacted chlorine groups at the surface after their synthesis (Table 3). These chlorine groups could be used for the post-functionalization of the HCCP-biphenol films with any monofunctional nucleophile that is able to undergo nucleophilic substitution with the chlorine groups of HCCP.

Fig. 9 shows top-view scanning electron micrographs before (Fig. 9a and b) and after (Fig. 9c and d) post-functionalization of a HCCP-BPH film with 2,2,2-trifluoroethanol (TFE). The use of a fluorine containing nucleophile provides contrast in elemental analysis techniques such as XPS. The surface morphology of both the aqueous and organic side of the film does not seem to change significantly upon post-functionalization.

The presence of TFE on the surface of the films can be proven by, for example, energy dispersive X-ray spectroscopy

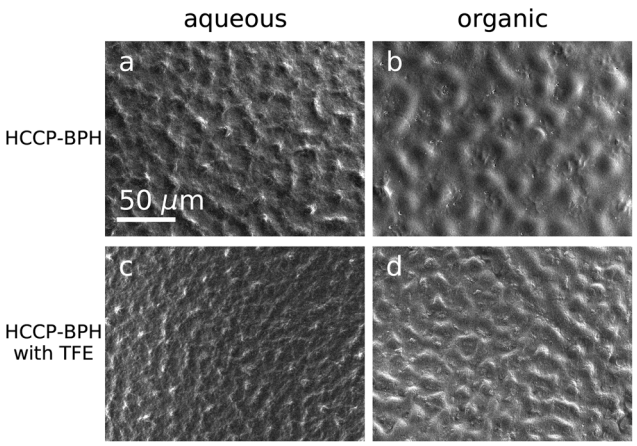

Fig. 9 Top-view scanning electron micrographs of (a, b) a HCCP-BPH film, and (c, d) a HCCP-BPH film functionalized with 2,2,2-trifluoroethanol.

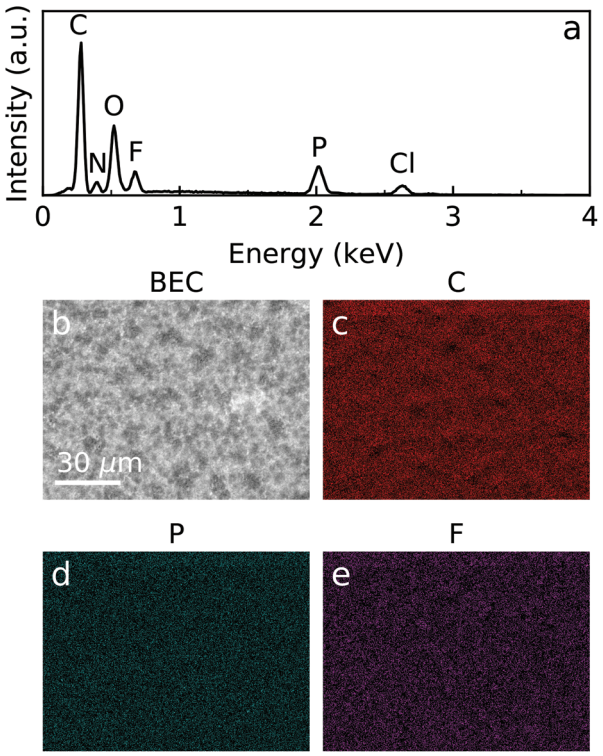

Fig. 10 (a) EDX spectrum, (b) back-scatter scanning electron micrograph, (c–e) EDX maps of the elements C, P, and F taken on the aqueous side of a HCCP-film functionalized with 2,2,2-trifluoroethanol.

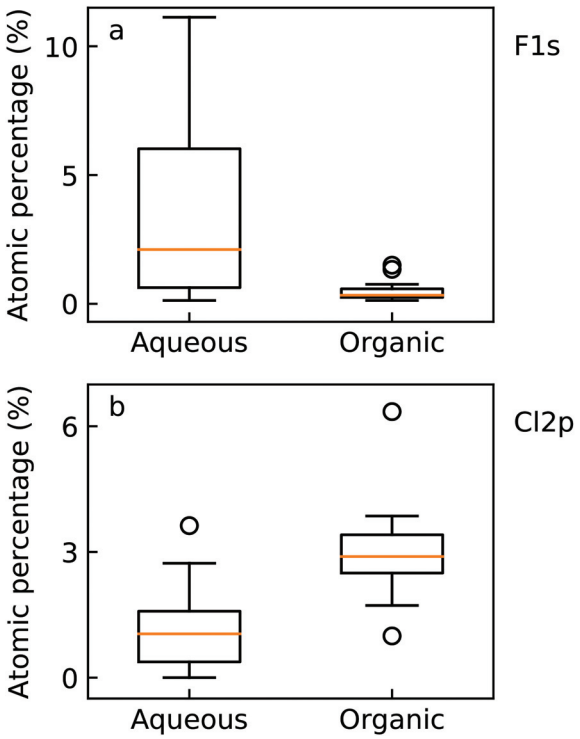

Fig. 11 Atomic percentages of (a) fluorine and (b) chlorine measured by XPS at both the aqueous and organic side of a HCCP-BPH film functionalized with 2,2,2-trifluoroethanol. All box plots were constructed from data obtained at 24 different spots.

(EDX). Fig. 10a shows such an EDX spectrum of the aqueous side of a TFE functionalized HCCP-BPH film. A clear peak belonging to the fluorine atoms of TFE is present at 0.7 keV. Additionally, Fig. 10b–e shows a back-scatter scanning electron micrograph and EDX maps of the elements C, P, and F, respectively. It can be concluded that the fluorine atoms are uniformly distributed at the interface (with a thickness of the EDX penetration depth) of the post-functionalized HCCP-BPH film.

XPS measurements reveal more insight on the concentration of elements at the surface of the film. Fig. 11 shows the difference in fluorine and chlorine content at the surface of the aqueous and the organic side of the functionalized film. The aqueous side of the film, that has been in contact with TFE, possesses a broadly distributed atomic concentration of fluorine, indicating the successful post-functionalization. In contrast, only minor traces of fluorine are present at the organic side of the film. The chlorine concentration shows a contrary trend; the aqueous side of the film possesses a lower concentration of chlorine as compared to the organic side. This is explained by the conversion of chlorine side-groups to TFE side-groups during the post-functionalization reaction. To conclude, the EDX and XPS results indicate the possibility of post-functionalizing these HCCP-biphenol films, thereby altering the surface properties. Of course this is not limited to TFE, but a wide range of mono-functional nucleophiles could be used.

4. Conclusion

We showed a simple and fast preparation of hybrid cyclomatrix polyphosphazene films made by interfacial polymerization, and provided a detailed characterization of the films obtained. Different aromatic biphenols were used, resulting in films with different cross-link densities and hence different mechanical properties. The pK_a of the biphenol is found to be an important parameter to tune the film properties. A lower pK_a results in a higher cross-link density and yielded films with a smooth surface morphology and high Young's moduli, whereas a high pK_a results in rough surface morphology and moderate Young's moduli.

The unreacted chlorine groups present at the surface allow for further post-functionalization of these films with a monofunctional nucleophile. Here, we showed the successful post-functionalization of a HCCP-BPH film with 2,2,2-trifluoroethanol.

Conflicts of interest

There are no conflicts to declare.

Acknowledgements

This work took place within the framework of the Institute for Sustainable Process Technology (ISPT, project BL-20-02) and by

the MESA+ Institute of Nanotechnology at the University of Twente.

The authors thank Joachim Roes from DWI – Leibniz-Institut für Interaktive Materialien (Aachen Germany) and Gerard Kip from the MESA+ Institute of Nanotechnology at the University of Twente for performing the XPS measurements.

References

1 G. Kickelbick, *Prog. Polym. Sci.*, 2003, **28**, 83–114.
2 G. L. Drisko and C. Sanchez, *Eur. J. Inorg. Chem.*, 2012, **2012**, 5097–5105.
3 H. R. Allcock, *Adv. Mater.*, 1994, **6**, 106–115.
4 H. R. Allcock, *Chemistry and Applications of Polyphosphazenes*, John Wiley & Sons, 2002.
5 S. Rothemund and I. Teasdale, *Chem. Soc. Rev.*, 2016, **45**, 5200–5215.
6 I. Manners, H. R. Allcock, G. Renner and O. Nuyken, *J. Am. Chem. Soc.*, 1989, **111**, 5478–5480.
7 R. Jaeger, M. Debowski, I. Manners and G. J. Vancso, *Inorg. Chem.*, 1999, **38**, 1153–1159.
8 V. Chandrasekhar, *Inorganic and Organometallic Polymers*, Springer Berlin Heidelberg, 2005.
9 H. R. Allcock, *Appl. Organomet. Chem.*, 2010, **24**, 600–607.
10 H. R. Allcock, *Soft Matter*, 2012, **8**, 7521–7532.
11 J. Köhler, S. Kühl, H. Keul, M. Möller and A. Pich, *J. Polym. Sci., Part A: Polym. Chem.*, 2014, **52**, 527–536.
12 D. Kumar, G. M. Fohlen and J. A. Parker, *Macromolecules*, 1983, **16**, 1250–1257.
13 D. Mathew, C. R. Nair and K. Ninan, *Polym. Int.*, 2000, **49**, 48–56.
14 J. Zhou, L. Meng, X. Feng, X. Zhang and Q. Lu, *Angew. Chem., Int. Ed.*, 2010, **49**, 8476–8479.
15 W. Wei, X. Huang, K. Chen, Y. Tao and X. Tang, *RSC Adv.*, 2012, **2**, 3765–3771.
16 D. Kumar, *Int. J. Adhes. Adhes.*, 1998, **18**, 109–113.
17 W. Wei, X. Huang, X. Zhao, P. Zhang and X. Tang, *Chem. Commun.*, 2010, **46**, 487–489.
18 Z. Huang, F. Zheng, S. Chen, X. Lu, C. G. Catharina Elizabeth van Sittert and Q. Lu, *RSC Adv.*, 2016, **6**, 75552–75561.
19 P. Vandezande, L. E. M. Gevers and I. F. J. Vankelecom, *Chem. Soc. Rev.*, 2008, **37**, 365–405.
20 W. Lau, A. Ismail, N. Misdan and M. Kassim, *Desalination*, 2012, **287**, 190–199.
21 M. J. Raaijmakers and N. E. Benes, *Prog. Polym. Sci.*, 2016, **63**, 86–142.
22 T. N. Thompson, S. Ramos-Hunter, J. Robertson and N. Y. Arnett, *Tetrahedron Lett.*, 2013, **54**, 5311–5313.
23 Y. W. Chen-Yang, S. J. Cheng and B. D. Tsai, *Ind. Eng. Chem. Res.*, 1991, **30**, 1314–1319.
24 L. Zhu, Y. Xu, W. Yuan, J. Xi, X. Huang, X. Tang and S. Zheng, *Adv. Mater.*, 2006, **18**, 2997–3000.
25 L. Zhu, Y. Zhu, Y. Pan, Y. Huang, X. Huang and X. Tang, *Macromol. React. Eng.*, 2007, **1**, 45–52.
26 Y. Zhu, X. Huang, W. Li, J. Fu and X. Tang, *Mater. Lett.*, 2008, **62**, 1389–1392.
27 J. Fu, Q. Xu, J. Chen, Z. Chen, X. Huang and X. Tang, *Chem. Commun.*, 2010, **46**, 6563–6565.
28 W. Wei, R. Lu, H. Xie, Y. Zhang, X. Bai, L. Gu, R. Da and X. Liu, *J. Mater. Chem. A*, 2015, **3**, 4314–4322.
29 P. Schön, K. Bagdi, K. Molnár, P. Markus, B. Pukánszky and G. J. Vancso, *Eur. Polym. J.*, 2011, **47**, 692–698.
30 H. Gojzewski, B. Imre, C. Check, R. Chartoff and J. Vancso, *J. Polym. Sci., Part B: Polym. Phys.*, 2016, **54**, 2298–2310.
31 J. L. Hutter and J. Bechhoefer, *Rev. Sci. Instrum.*, 1993, **64**, 1868–1873.
32 J. E. Sader, I. Larson, P. Mulvaney and L. R. White, *Rev. Sci. Instrum.*, 1995, **66**, 3789–3798.
33 H.-J. Butt, B. Cappella and M. Kappl, *Surf. Sci. Rep.*, 2005, **59**, 1–152.
34 B. Cappella and G. Dietler, *Surf. Sci. Rep.*, 1999, **34**, 1–104.
35 Bruker, *PeakForce QNM User Guide*, 2011.
36 H. Gojzewski, M. Sadej, E. Andrzejewska and M. Kokowska, *Eur. Polym. J.*, 2017, **88**, 205–220.
37 Z. Wang, A. A. Volinsky and N. D. Gallant, *J. Appl. Polym. Sci.*, 2014, **131**, 41050.
38 D. W. Scott, *Biometrika*, 1979, **66**, 605–610.
39 M. J. T. Raaijmakers, E. J. Kappert, A. Nijmeijer and N. E. Benes, *Macromolecules*, 2015, **48**, 3031–3039.
40 ChemAxon, Chemicalize, https://chemicalize.com/welcome, 2017.
41 J. Reijenga, A. van Hoof, A. van Loon and B. Teunissen, *Anal. Chem. Insights*, 2013, **8**, 53–71.
42 R. Sydam and M. Deepa, *J. Mater. Chem. C*, 2013, **1**, 7930–7940.
43 A. K. Ghosh, B.-H. Jeong, X. Huang and E. M. Hoek, *J. Membr. Sci.*, 2008, **311**, 34–45.
44 B. Khorshidi, T. Thundat, B. A. Fleck and M. Sadrzadeh, *Sci. Rep.*, 2016, **6**, 22069.
45 Y. Zhang, N. E. Benes and R. G. H. Lammertink, *Lab Chip*, 2015, **15**, 575–580.
46 H.-J. Butt and M. Kappl, *Adv. Colloid Interface Sci.*, 2009, **146**, 48–60.
47 A. Ptak, H. Gojzewski, M. Kappl and H.-J. Butt, *Chem. Phys. Lett.*, 2011, **503**, 66–70.
48 J. F. Moulder, W. F. Stickle, P. E. Sobol and K. D. Bomben, *Handbook of X-ray Photoelectron Spectroscopy*, PerkinElmer Corporation, 1992.
49 Z. Chen, J. Fu, M. Wang, X. Wang, J. Zhang and Q. Xu, *Appl. Surf. Sci.*, 2014, **289**, 495–501.
50 S. J. Maynard, T. R. Sharp and J. F. Haw, *Macromolecules*, 1991, **24**, 2794–2799.
51 M. E. Gouri, A. E. Bachiri, S. E. Hegazi, M. Rafik and A. E. Harfi, *Polym. Degrad. Stab.*, 2009, **94**, 2101–2106.
52 Y. W. Chen-Yang, J. S. Jiang, Y. W. Ho and S. J. Cheng, *J. Inorg. Organomet. Polym.*, 1992, **2**, 243–254.

